Gene Therapy (2015) **22**, 503–515

www.nature.com/gt

ORIGINAL ARTICLE

Ameliorating pathogenesis by removing an exon containing a missense mutation: a potential exon-skipping therapy for laminopathies

J Scharner, N Figeac, JA Ellis and PS Zammit

Exon skipping, as a therapy to restore a reading frame or switch protein isoforms, is under clinical trial. We hypothesised that removing an in-frame exon containing a mutation could also improve pathogenic phenotypes. Our model is laminopathies: incurable tissue-specific degenerative diseases associated with *LMNA* mutations. *LMNA* encodes A-type lamins, that together with B-type lamins, form the nuclear lamina. Lamins contain an alpha-helical central rod domain composed of multiple heptad repeats. Eliminating *LMNA* exon 3 or 5 removes six heptad repeats, so shortens, but should not otherwise significantly alter, the alpha-helix. Human Lamin A or Lamin C with a deletion corresponding to amino acids encoded by exon 5 (Lamin A/C-Δ5) localised normally in murine *lmna*-null cells, rescuing both nuclear shape and endogenous Lamin B1/emerin distribution. However, Lamin A carrying pathogenic mutations in exon 3 or 5, or Lamin A/C-Δ3, did not. Furthermore, Lamin A/C-Δ5 was not deleterious to wild-type cells, unlike the other Lamin A mutants including Lamin A/C-Δ3. Thus Lamin A/C-Δ5 function as effectively as wild-type Lamin A/C and better than mutant versions. Antisense oligonucleotides skipped *LMNA* exon 5 in human cells, demonstrating the possibility of treating certain laminopathies with this approach. This proof-of-concept is the first to report the therapeutic potential of exon skipping for diseases arising from missense mutations.

Gene Therapy (2015) **22,** 503–515; doi:10.1038/gt.2015.8; published online 2 April 2015

INTRODUCTION

A promising form of RNA therapeutics is antisense oligonucleotides (AONs)-mediated 'exon skipping'.[1,2] Mechanistically, AONs mask splice sites or splice enhancer regions, thus preventing access of the splicing machinery to the target exon, which results in exon skipping. AONs are currently in clinical trial for Duchenne muscular dystrophy (DMD; MIM 310200) to correct disrupted reading frames by deleting an exon(s) to generate an internally deleted, but in-frame, novel transcript encoding a modified protein with functionality.[3,4] Importantly, in-frame mutations in the *DMD* gene cause the generally milder Becker muscular dystrophy (MIM 300376), so both guiding exon selection and demonstrating the potential of truncated dystrophin species to alleviate symptoms in DMD.[5] Other applications of AONs include exon inclusion to restore protein function (for example, spinal muscular atrophy (SMA), MIM 253300),[6] blocking *de novo*/cryptic splice sites to restore correct splicing (for example, Hutchison–Gilford progeria syndrome (HGPS), MIM 176670 and β-thalassemia, MIM 613985)[7] or to disrupt protein expression by removing an exon containing a polyA signal (for example, facioscapulohumeral muscular dystrophy, MIM 158900).[8]

Our model is laminopathies, comprising ~16 tissue-specific degenerative diseases, including muscular dystrophies such as Emery–Dreifuss muscular dystrophy (EDMD, MIM 181350), limb–girdle muscular dystrophy 1B (LGMD1B, MIM 159001) and congenital muscular dystrophy (L-CMD, MIM 613205); dilated cardiomyopathy (DCM, MIM 115200); peripheral neuropathies, mainly autosomal recessive Charcot–Marie–Tooth disease type 2 (AR-CMT2A, MIM 605588); familial partial lipodystrophy type 2 (FPLD2, MIM 151660) and premature ageing syndromes such as HGPS.[9,10] Laminopathies generally arise from autosomal-dominant gain-of-function mutations in *LMNA* (MIM 150330), being either missense or nonsense mutations, or mutations that affect splicing to cause abnormal posttranslational processing to generate progerin, causing HGPS.[11]

LMNA encodes A-type nuclear lamins, predominately Lamin A and Lamin C. *LMNB1* and *LMNB2* encode the B-type lamins, lamin B1 and lamin B2 respectively. A-type and B-type lamins are type V intermediate filaments, which together form a proteinaceous meshwork underlying the inner nuclear membrane, termed the nuclear lamina.[12] The nuclear lamina provides structural support for the nuclear membrane and connects the nucleus to the cytoskeleton via the LINC complex, as well as having important roles in chromatin organisation, gene expression, DNA repair and mitosis.[13,14] Features of laminopathies include dysmorphic nuclei, protein mislocalisation (for example, Lamin B1) and deregulation of gene expression.[15] Pathogenic characteristics can be modelled by retroviral-mediated expression of mutant Lamin A/C proteins *in vitro*.[16]

Lamin A and/or Lamin C are expressed in most cell types, yet many disorders caused by *LMNA* mutations are tissue-specific.[10] A possible explanation for this tissue-restricted pathology is through perturbed interactions of lamins with tissue-specific binding partner proteins/isoforms in the nuclear envelope and beyond, for example, via the LINC complex.[17,18]

Existing treatments for laminopathies are palliative, but drugs acting directly on, or downstream of, Lamin A/C are in development, particularly for HGPS (for example, rapamycin[19]

Randall Division of Cell and Molecular Biophysics, King's College London, London, UK. Correspondence: Professor PS Zammit, Randall Division of Cell and Molecular Biophysics, King's College London, London SE1 1UL, UK.
E-mail: peter.zammit@kcl.ac.uk
Received 9 September 2014; revised 18 December 2014; accepted 30 December 2014; published online 2 April 2015

and farnesyltransferase inhibitors[20]) and DCM (mitogen-activated protein kinase inhibitors[21]). Stem cell-based approaches coupled with homologous recombination-based gene correction are also in development.[22] Finally, manipulation of other genes may compensate for Lamin A/C deficiency (or the presence of mutant Lamin A/C), for example, we recently reported an improved phenotype in the *Lmna*-null mouse by knocking out *Lap2a*.[23]

As current treatments for laminopathies are palliative, novel therapeutic approaches are needed. *LMNA* is alternatively spliced to generate four isoforms (A, A-Δ10, C and C2), suggesting that it is tolerant to re-directed splicing.[13] Indeed, AONs effectively block aberrant splice sites used to generate progerin, so reducing levels and alleviating the associated phenotype.[24] However, there is no treatment that corrects/bypasses missense, insertions/deletions or nonsense mutations in patients.

Here we investigated whether eliminating a *Lmna* exon containing a mutation improves a pathogenic phenotype. In theory, having an internally truncated Lamin A/C protein lacking amino acids encoded by an in-frame exon carrying a mutation will be relatively benign if the lost amino acids are not essential to protein function, as compared with having the complete protein carrying the pathogenic mutation. We found that human Lamin A/C with a deletion corresponding to amino acids encoded by exon 5 localised normally in murine *lmna*-null cells and rescued both nuclear shape and distribution of endogenous Lamin B1 and emerin. We then demonstrate the feasibility of using AONs to skip *LMNA* exon 5 in human cells, as a possible treatment for laminopathies arising from mutations in *LMNA* exon 5 (Table 1).

This study provides a proof-of-concept that exon skipping can be used to treat diseases arising from missense mutations in proteins possessing a repeating and partially redundant domain, such as found in Lamin A/C. Furthermore, such therapy is also potentially applicable to a range of similarly structured proteins with pathogenic missense or other point mutations, small deletions, insertions or duplications.

RESULTS

Selection of *LMNA* exons for therapeutic skipping

Complete deficit of A-type lamins is lethal in man[25] and drastically shortens lifespan in mouse,[26] so in-frame *LMNA* transcripts are needed, thus excluding removal of *LMNA* exons 1, 2, 6 or 7 (Figure 1a). *LMNA* exon 9 was not considered as its removal is associated with a progeroid phenotype in mice[27] while deletion of exon 11 occurs in patients with restrictive dermopathy (MIM 275210).[28] Similarly, exon 4 encodes the flexible linker region between coil 1 and 2 (L12) and exons 8 and 10 encode parts of the Ig-fold domain, important for protein interactions and possible lamin filament assembly.[18,29] Exon 10 also encodes the C-terminus of Lamin C.

Nuclear lamins have an α-helical central rod domain composed of multiple heptad repeats (Figure 1b). We predicted that removal of complete heptad repeats would not disrupt assembly of α-helical coiled coils, and *LMNA* exons 3 and 5 each encode six complete heptad repeats located in coils 1B and 2B, respectively. Crucially, cytoplasmic intermediate filament proteins lack six heptad repeats in the central rod domain and assemble correctly with this shortened configuration (Figure 1c). Furthermore, deletion of *LMNA* exon 3 or 5 does not affect linker or hinge regions, nor the intermediate filament consensus sequence, of the encoded proteins (Figures 1a and c).

Table 1. Frequency and associated phenotypes of mutations in *LMNA* exon 5

Mutation	*Reported cases*	*Disease*[a]	*Percentage of total reports*[b]
p.L271P	3	EDMD	0.13
p.S277P	1	EDMD	0.04
p.A278T	5	LGMD1B	0.22
p.E291K	1	DCM-CD	0.04
p.L292P	2	LGMD1B/L-CMD	0.09
p.Q294P	2	EDMD	0.09
p.S295P	1	EDMD	0.04
p.R298C[c]	80	AR-CMT2A	3.55
p.I299V	4	FPLD	0.18
p.D300N	3	Werner syndrome	0.13
p.D300G	1	Progeroid syndrome	0.04
p.L302P	1	L-CMD	0.04
p.S303P	3	LGMD1B	0.13
p.K311R	2	LGMD1B	0.09
p.Q312H	2	LGMD1B/DCM-CD	0.09
p.A287LfsX193	1	LGMD1B	0.04
p.A287RfsX44	1	DCM-CD	0.04
p.A287VfsX193	1	DCM-CD	0.04
p.A289RfsX190	2	LGMD1B	0.09
p.S303CfsX27	16	LGMD1B	0.71
	132		5.86

Abbreviations: AR-CMT2A, autosomal recessive Charcot–Marie–Tooth disease type 2; DCM-CD, conduction disease associated with dilated cardiomyopathy; EDMD, Emery–Dreifuss muscular dystrophy; FPLD, familial partial lipodystrophy type 2; L-CMD, Lamin A/C-related congenital muscular dystrophy; LGMD1B, limb–girdle muscular dystrophy 1B. [a]Phenotype reported in the majority of patients. [b]2251 reported cases (http://www.umd.be/LMNA/). [c]Recessive mutation.

Figure 1. Exon/intron structure of the *LMNA* gene and organisation of encoded Lamin A/C proteins. (**a**) The *LMNA* gene consists of 12 exons and encodes Lamin A and Lamin C, and minor isoforms A-Δ10 and C2. Lamin A is alternatively spliced from exon 10, while the stop codon for Lamin C is in exon 10. The amino acids encoded by an exon are given above the respective exon. Dotted lines indicate amino acids and regions of the protein encoded by each exon. All *LMNA* exons except exons 1, 2, 6 and 7 can be removed without affecting the open reading frame (NLS: nuclear localisation signal). (**b**) Two representative consecutive heptad repeats (residues 338–351) from coil 2B of the central rod domain of human Lamin A are shown (PDB 1X8Y[55]). Sequences of α-helical coiled-coils display a periodicity of seven amino acids (heptad repeats) with nonpolar amino acids occupying heptad positions a and d. Occasionally, charged amino acids are located on position a or d such as lysine 341, which forms a salt bridge with a glutamate residue of the neighbouring α-helix, reinforcing the coiled coil. (**c**) Amino-acid sequence of the central rod domain of eight different human intermediate filaments were obtained from the UniProt protein sequence database and aligned using Clustal2W. Coils 1a, 1b, 2a and 2b and linker regions L1, L12 and L2 are indicated above the sequence. The heptad repeat position for each residue (a–g) and the intermediate filament IF consensus sequences (boxed) are also indicated (adapted from Herrmann and Aebi[56]). The amino acids encoded by *LMNA* exons 3 and 5 are in red text and underlined; NF-L, Neurofilament light; (.) semi-conserved; (:) conserved; (*) identical. (**d**) Human Lamin A constructs used were: full length wild-type Lamin A (Lamin A-wt), Lamin A with amino acids encoded by exon 3 deleted (Lamin A-Δ3) and Lamin A with amino acids encoded by exon 5 deleted (Lamin A-Δ5) and four full-length Lamin A constructs with pathogenic point mutations encoded by exon 3 (Lamin A-R190dup or Lamin A-N195K) or exon 5 (Lamin A-S295P or Lamin A-S303P). (**e** and **f**) Western blotting of wild-type or *lmna*-null pMEFs infected with retroviruses encoding each of the human Lamin A constructs shows that their sizes are correct, expression levels are consistent with endogenous murine Lamin A/C levels and production of eGFP from the *IRES-eGFP* in the retroviral backbone. β-Tubulin served as a loading control.

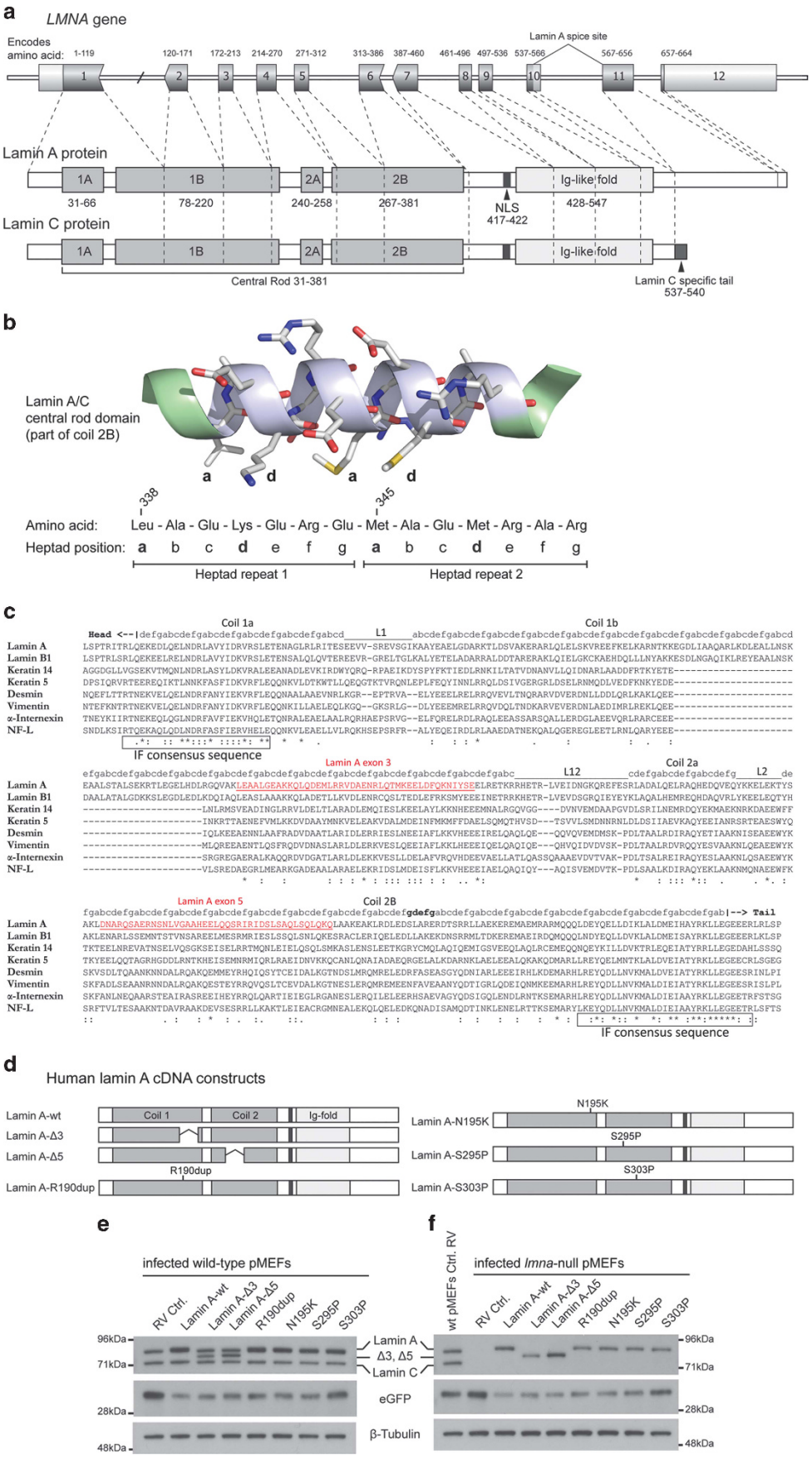

Human Lamin A-Δ5 localises correctly in the nucleus

We produced retroviruses encoding wild-type human Lamin A (Lamin A-wt), human lamin-A lacking amino acids encoded by exon 3 (Lamin A-Δ3) or exon 5 (Lamin A-Δ5) or human Lamin A variants containing known pathogenic mutations encoded by exon 3 (Lamin A-R190dup or Lamin A-N195K) or exon 5 (Lamin A-S295P or Lamin A-S303P—Table 1) (Figure 1d). Each Lamin A construct was encoded with enhanced green fluorescent protein (eGFP) from an *IRES* in the retroviral backbone, to facilitate identification of infected cells. Western blotting analysis of infected wild-type (Figure 1e) or *lmna*-null primary murine embryonic fibroblasts (pMEFs) (Figure 1f) showed

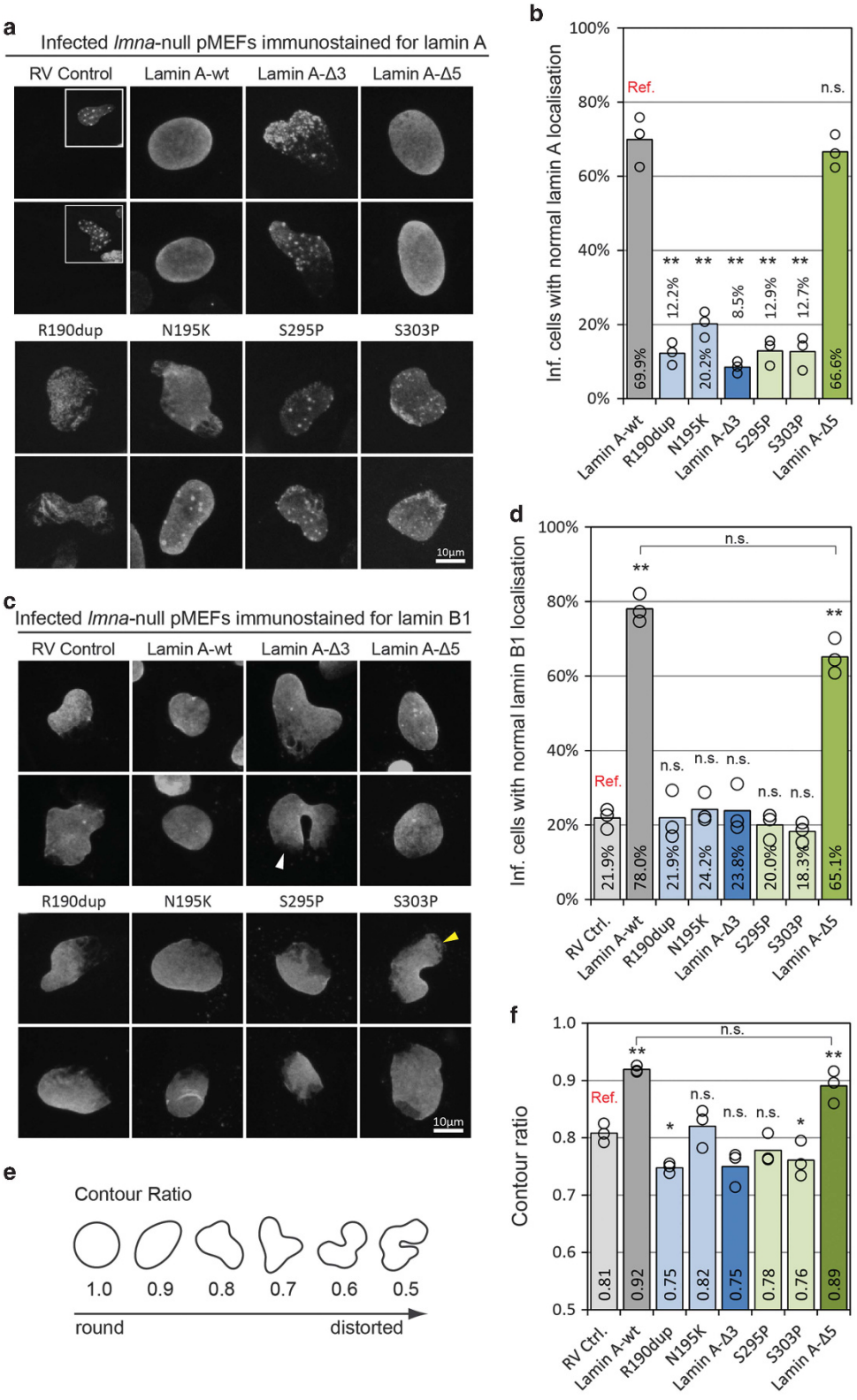

retroviral-mediated expression levels consistent with native murine Lamin A/C in wild-type cells, together with eGFP expression.

Human Lamin A can rescue the nuclear phenotype in *lmna*-null cells, as 3 days after retroviral infection, Lamin A-wt was localised at the nuclear lamina and in the nucleoplasm of eGFP +ve infected *lmna*-null pMEFs (Figure 2a). Furthermore, both the characteristic endogenous murine Lamin B1 mislocalisation and nuclear deformation of *lmna*-null cells were normalised by exogenous Lamin A-wt (Figure 2).

Comparison with rescue by Lamin A-wt was used to test whether Lamin A-Δ3 or Lamin A-Δ5 could also rescue nuclear abnormalities in *lmna*-null cells and how they compare to the *LMNA* variants with missense mutations/duplications in *LMNA* exons 3 or 5. After 3 days of expression, an average of 69.9% of eGFP+ve *lmna*-null pMEFs infected with Lamin A-wt had an even Lamin A distribution throughout the nucleus, which was not significantly different from the mean proportion of *lmna*-null cells expressing Lamin A-Δ5 with correct localisation (66.6%; Figures 2a and b). By contrast, the Lamin A variants with point mutations/duplications in regions encoded by *LMNA* exon 3 or 5 were unable to localise correctly in eGFP+ve *lmna*-null pMEFs (Figures 2a and b). Nuclei in these eGFP+ve cells demonstrated abnormalities such as Lamin A aggregation, capping and honeycomb structures (Figure 2a). Lamin A-Δ3 was also unable to localise correctly in *Lmna*-null cells, with abnormal aggregation into nucleoplasmic foci and prominent Lamin A capping (Figures 2a and b).

Endogenous Lamin B1 localisation in *lmna*-null cells restored by human Lamin A-Δ5

Nuclei of *lmna*-null pMEFs show a range of abnormalities, including severe morphological deformations, Lamin B capping and loss of emerin localisation from the nuclear rim.[26] Re-introduction of Lamin A-wt into *lmna*-null cells can reverse these abnormalities (Figures 2c, d and 3).[26] Therefore, we tested whether Lamin A variants containing exon deletions can also rescue these hallmarks of pathogenesis.

The first effect analysed was potential rescue of endogenous murine Lamin B1 capping and honeycomb structures in *lmna*-null pMEFs by Lamin A variants (Figures 2c and d). In *lmna*-null pMEFs infected with control RV, only 21.9% of nuclei had normal localisation of endogenous Lamin B1 (Figures 2c and d). Expression of wild-type Lamin A-wt increased this proportion to 78.0% ($P < 0.001$), while introduction of Lamin A variants with point mutations/duplications in exon 3 or 5, or Lamin A-Δ3, were unable to normalise murine Lamin B1 localisation in eGFP+ve *lmna*-null pMEFs (Figures 2c and d). In comparison, Lamin A-Δ5 expression led to an increased proportion (65.1%) of *lmna*-null pMEFs with normal endogenous Lamin B1 distribution. This was a significant improvement over both control RV-infected cells ($P < 0.01$), and Lamin A variants with a point mutation in exon 5 (Lamin A-S295P ($P < 0.001$) or Lamin A-S303P ($P < 0.01$) (Figure 2d)).

Human Lamin A-Δ5 rescues nuclear shape in *lmna*-null cells

Lmna-null cells are characterised by nuclear deformations, which can be measured by the contour ratio (CR). A cartoon of nuclei with different degrees of deformations and their corresponding contour ratio is shown for reference (Figure 2e). *Lmna*-null pMEFs infected with control RV had an average contour ratio of 0.81 (Figure 2f), which corresponds to clear deformation (Figure 2e). Introduction of Lamin A-wt led to a significant increase in the mean contour ratio to 0.92, corresponding to a more characteristic ovoid shape (Figure 2f). Lamin A-R190dup (CR = 0.75), Lamin A-S303P (CR = 0.76) or Lamin A-Δ3 (CR = 0.75) significantly decreased the mean contour ratio, while Lamin A-N195K (CR = 0.82) or Lamin A-S295P (CR = 0.78) had no effect (Figure 2f). Importantly, Lamin A-Δ5 increased the mean contour ratio (CR 0.89) of eGFP+ve *lmna*-null cells to that of cells infected with Lamin A-wt (Figure 2f).

Endogenous emerin localisation in *lmna*-null cells restored by human Lamin A-Δ5

Lmna-null cells show a redistribution of emerin from the nuclear envelope to the endoplasmic reticulum (ER)[30] (Figure 3a). Expression of Lamin A-Δ3 did not alter this mislocalisation in *Lmna*-null pMEFs, but expression of Lamin A-wt or Lamin A-Δ5 led to normalisation of endogenous murine emerin to the nuclear membrane. This change in emerin localisation was quantified by measuring the fluorescence intensity of emerin immunostaining across an infected eGFP+ve cell and comparing it to a neighbouring uninfected cell (Figures 3b and c). Non-infected eGFP-ve *lmna*-null pMEFs exhibit strong emerin immunostaining beyond the nucleus, which most likely represents emerin in the ER (yellow box in Figures 3b and c). However, most emerin immunostaining was clearly confined to the nucleus in eGFP+ve cells infected with Lamin A-wt (red box in Figure 3b) or Lamin A-Δ5 (red box in Figure 3c).

Human Lamin A-Δ5 does not have a deleterious effect on wild-type pMEFs

Most pathogenic *LMNA* mutations are dominant, so we also tested the effects of Lamin A variants in wild-type pMEFs to simulate a heterozygous phenotype. Only a mean of 23.1% of nuclei in wild-type pMEFs had slight abnormalities in Lamin A/C localisation. Retroviral-mediated expression of Lamin A-wt did not have a negative effect on Lamin A/C localisation (Figures 4a and b).

Figure 2. Human Lamin A-Δ5 localises normally in *lmna*-null pMEFs and can rescue their abnormal nuclear morphology and protein localisation. (**a**) Representative micrographs of nuclei from eGFP+ve *lmna*-null pMEFs infected with retroviral constructs encoding different Lamin A variants and co-immunostained for Lamin A/C and eGFP (inserts shows DAPI-stained nuclei). (**b**) Mean percentage of *lmna*-null pMEFs that have a regular distribution of Lamin A throughout the nucleus and around the nuclear rim, as seen in wild-type pMEFs and *lmna*-null pMEFs expressing control native human Lamin A-wt. Only Lamin A-Δ5 localised correctly. Open circles represent values obtained from three independent *lmna*-null pMEF lines, with at least 230 nuclei in total analysed for each condition. (**c**) Representative micrographs of nuclei from eGFP+ve *lmna*-null pMEFs infected with retroviral constructs encoding different Lamin A variants immunostained for endogenous Lamin B1. Infection with only Lamin A-wt or Lamin A-Δ5 restores normal endogenous Lamin B1 localisation, while the other Lamin A mutants are unable to prevent Lamin B1 capping (arrowheads) and honeycomb structures (arrows). (**d**) Mean percentage of *lmna*-null pMEFs that have an even distribution of endogenous Lamin B1 throughout the nucleus and around the nuclear rim, showing that only Lamin A-wt or Lamin A-Δ5 restore mouse Lamin B1 localisation. Open circles represent values obtained from three independent *lmna*-null pMEF lines, with at least 280 nuclei in total analysed for each condition. (**e**) Cartoon depicting representative nuclear shapes and their corresponding contour ratio. As nuclei become more deformed, the contour ratio decreases. (**f**) Average contour ratio of nuclei from eGFP+ve *lmna*-null pMEFs after infection with retroviral constructs encoding different Lamin A variants, showing that only Lamin A-wt or Lamin A-Δ5 can restore nuclear shape. Open circles represent values obtained from three independent *lmna*-null pMEF lines, with at least 240 nuclei in total analysed for each condition. Significant difference from Lamin A-wt or control retrovirus infected cells as appropriate (Ref) using a two-tailed paired *t*-test is denoted by $*P < 0.05$ or $**P < 0.01$, while 'NS' indicates no significant change. Scale bar represents 10 μm.

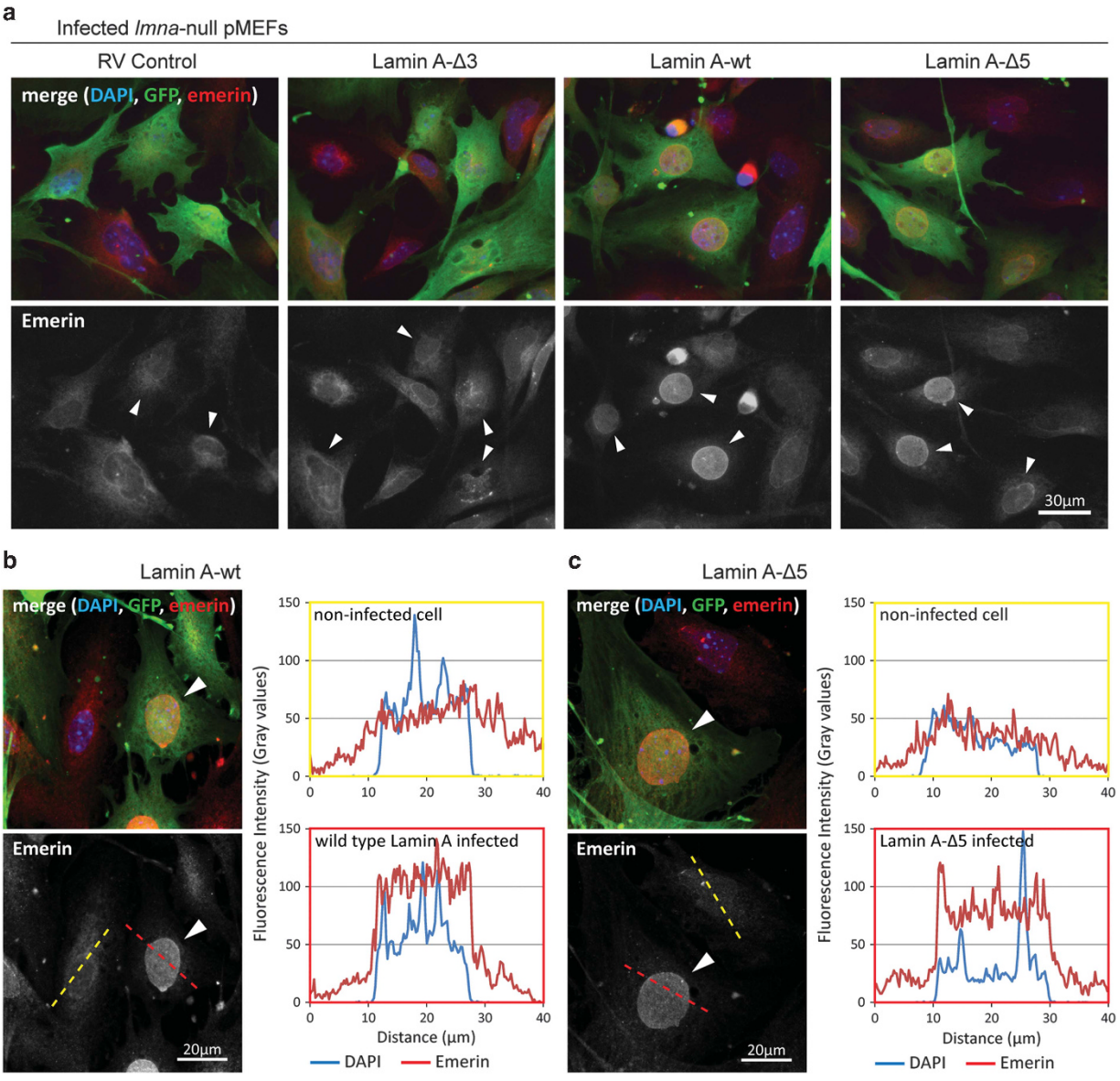

Figure 3. Normalisation of endogenous emerin localisation in *lmna*-null pMEFs expressing human Lamin A-Δ5. (**a**) Representative micrographs of eGFP+ve infected *lmna*-null pMEFs co-immunostained for endogenous emerin (red) and eGFP (green), with DAPI counterstaining (blue). Emerin immunostaining is shown in monochrome below the composite, with eGFP+ve infected cells indicated by white arrowheads. (**b** and **c**) Confocal images and fluorescence intensity plots of mouse emerin immunostaining across uninfected *lmna*-null pMEFs show that emerin is not concentrated to the nucleus, as demarcated by DAPI (yellow boxes). (**b**) Expression of Lamin A-wt causes endogenous emerin (red) to relocate to the nucleus of eGFP+ve cells (white arrowhead) as demarcated by DAPI (red box). (**c**) Infection with Lamin A-Δ5 encoding retrovirus also restores emerin (red) distribution to the nucleus as shown in the confocal image and fluorescence intensity plots (red box) of the eGFP+ve *lmna*-null pMEF (white arrowhead). Red and yellow dashed lines mark the track of the fluorescent intensity plot. Scale bar represents 30 μm for panel **a**, and 20 μm for panels **b** and **c**.

Nuclear aggregations of Lamin A, such as those seen in *lmna*-null pMEFs, were not observed in wild-type pMEFs after expression of any Lamin A variants. However, the mean proportion of cells with abnormal Lamin A/C localisation increased after expression of Lamin A-Δ3, Lamin A-R190dup, Lamin A-S295P or Lamin A-S303P, which mainly manifested as honeycomb structures (Figures 4a and b). Crucially, expression of Lamin A-Δ5 had no effect on the mean proportion of nuclei with abnormal Lamin A/C localisation, being comparable to Lamin A-wt-infected cells (Figures 4a and b).

The same was observed when analysing endogenous murine Lamin B1 localisation and contour ratio (Figures 4c–e). Lamin A-R190dup, Lamin A-S295P, Lamin A-S303P or Lamin A-Δ3 all increased both the mean proportion of nuclei with Lamin B1 abnormalities, including capping and honeycomb structures (Figures 4c and d), and reduced the average contour ratio, compared with Lamin A-wt-infected cells (Figure 4e). Importantly, endogenous Lamin B1 localisation and nuclear morphology were unaffected by Lamin A-Δ5 expression: both the mean proportion of eGFP+ve wild-type pMEFs with abnormal lamin B1 localisation (8.0%) and the average contour ratio (0.91) were not significantly different from control Lamin A-wt-infected cells (Figures 4c–e). However, with Lamin A-Δ5 infection, the percentage of cells with mislocalised Lamin B1 was significantly less, and the contour ratio was significantly higher, compared with the expression of either Lamin A-S295P ($P < 0.05$) or Lamin A-S303P ($P < 0.05$) (Figures 4d and e).

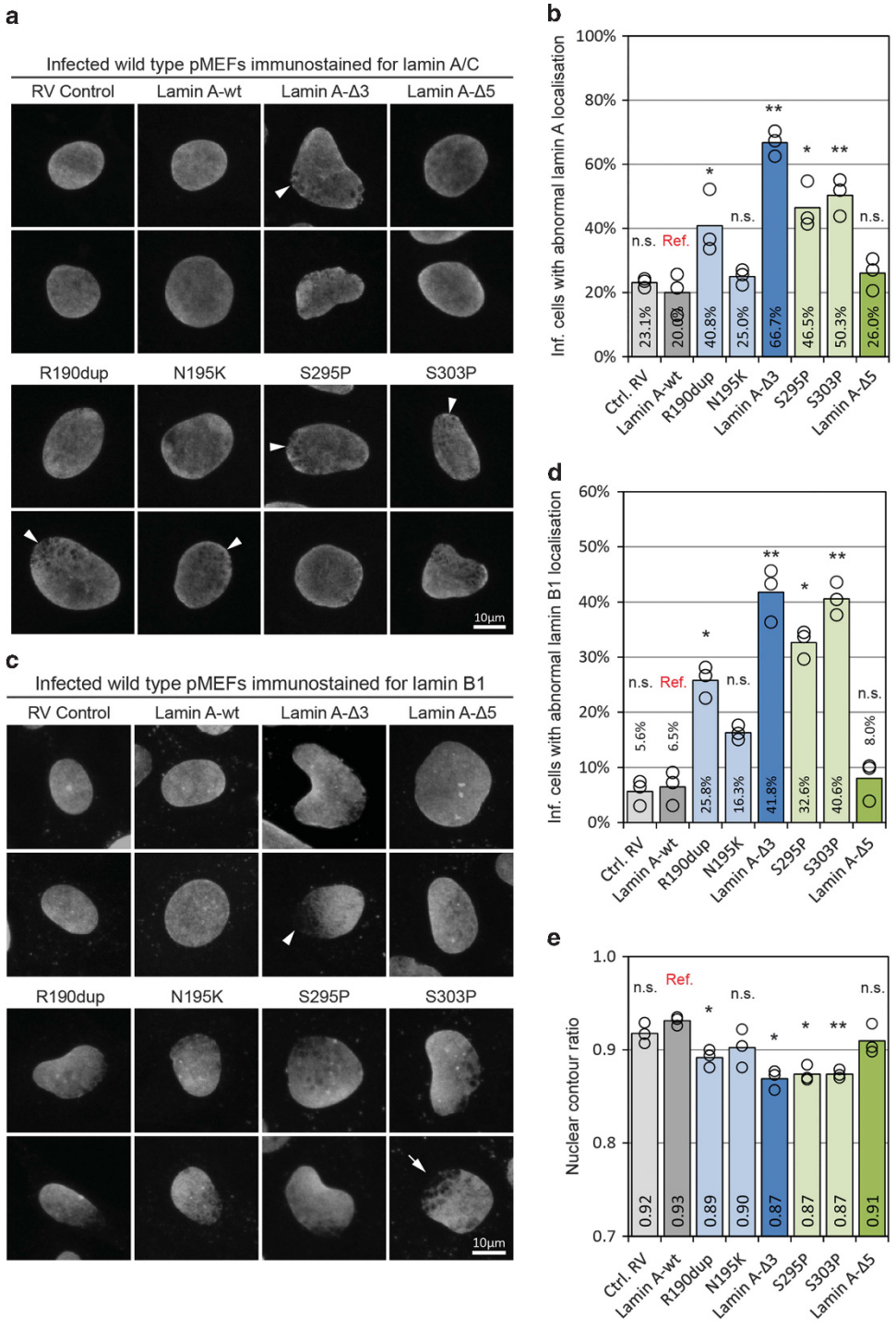

Figure 4. Human Lamin A-Δ5 does not have a dominant deleterious effect on lamin localisation and nuclear morphology in wild-type pMEFs. (**a**) Representative micrographs of nuclei of infected eGFP+ve wild-type pMEFs immunostained for Lamin A/C. Lamin A-N195K or Lamin A-Δ5 did not affect Lamin A/C localisation in eGFP+ve wild-type pMEFs. However, cells expressing Lamin A-Δ3, Lamin A-R190dup, Lamin A-S295P or Lamin A-S303P exhibited perturbations in Lamin A distribution, such as honeycomb structures (arrowheads). (**b**) Mean percentage of nuclei of eGFP+ve wild-type pMEFs showing abnormal Lamin A localisation (mainly honeycomb structures). Open circles represent values obtained from three independent wild-type pMEF lines, with at least 210 nuclei in total analysed for each condition. (**c**) Representative micrographs of nuclei from eGFP+ve wild-type MEFs infected with retroviral constructs encoding different Lamin A variants immunostained for Lamin B1. Lamin A-N195K or Lamin A-Δ5 did not affect Lamin B1 localisation, while the other Lamin A mutant versions did, with evident endogenous Lamin B1 capping (arrowhead), and/or honeycomb structures (arrow). (**d**) Mean percentage of eGFP+ve wild-type MEFs that show abnormalities in Lamin B1 localisation, such as capping and honeycomb structures. Open circles represent values obtained from three independent wild-type pMEF lines, with at least 260 nuclei in total analysed for each condition. (**e**) Average contour ratio of nuclei eGFP+ve infected cells shows that Lamin A-N195K or Lamin A-Δ5 did not affect nuclear shape, while the other Lamin A mutant versions did. Open circles represent values obtained from three independent wild-type pMEF lines, with at least 160 nuclei in total analysed for each condition. Significant difference from Lamin A-wt infected cells (Ref) using a two-tailed paired *t*-test is denoted by $*P < 0.05$ or $**P < 0.01$, while 'NS' indicates no significant change. Scale bar represents 10 μm.

Human Lamin C-Δ5 rescues the nuclear phenotype of *lmna*-null cells

LMNA predominately encodes Lamin A and Lamin C, expressed at similar levels in most tissues, but with exceptions such as in the brain.[31] As exon 5 is common to both Lamin A and Lamin C, exon skipping would affect translation into both isoforms. To analyse whether human Lamin C-Δ5 had similar beneficial effects as Lamin A-Δ5, we cloned human wild-type human Lamin C (Lamin C-wt), Lamin C-Δ3 and Lamin C-Δ5 encoding cDNA into *pMSCV-IRES-eGFP* (Figures 5a and b).

Lamin C protein localisation was normal in approximately half of all eGFP+ve *lmna*-null pMEFs infected with Lamin C-wt (54.2%) or Lamin C-Δ5 (49%). By contrast, Lamin C-Δ3 was mislocalised, exhibiting patchy immunostaining and aggregates, with only a mean of 9% of infected cells classified as normal (Figures 5c and d). This is consistent with our observations with Lamin A-Δ3. Abnormal localisation of endogenous murine Lamin B1 in many *lmna*-null pMEFs was also ameliorated by expression of either Lamin C-wt or Lamin C-Δ5 but not by Lamin C-Δ3 (Figures 5e and f). Similarly, endogenous emerin was also re-localised from the ER to

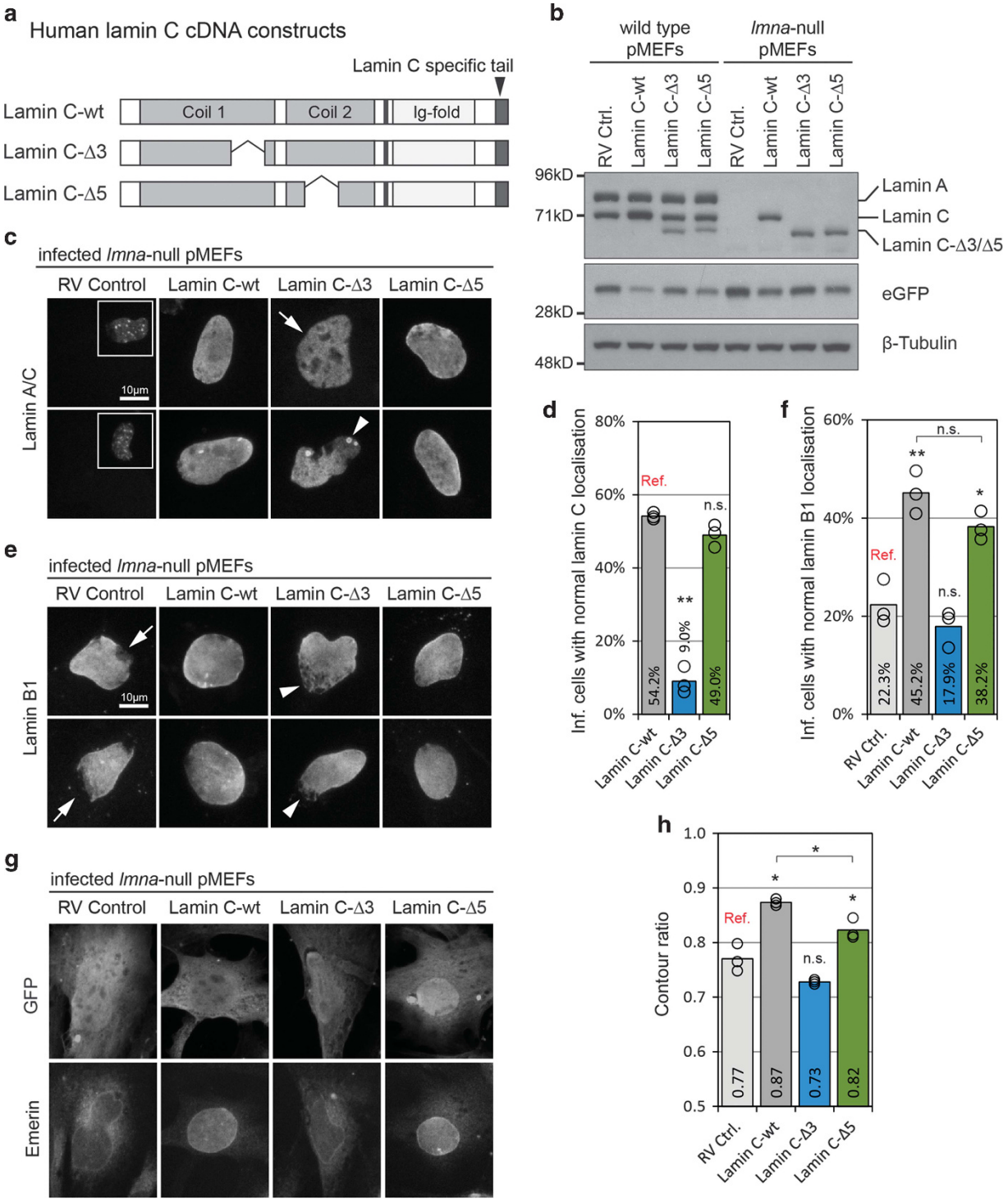

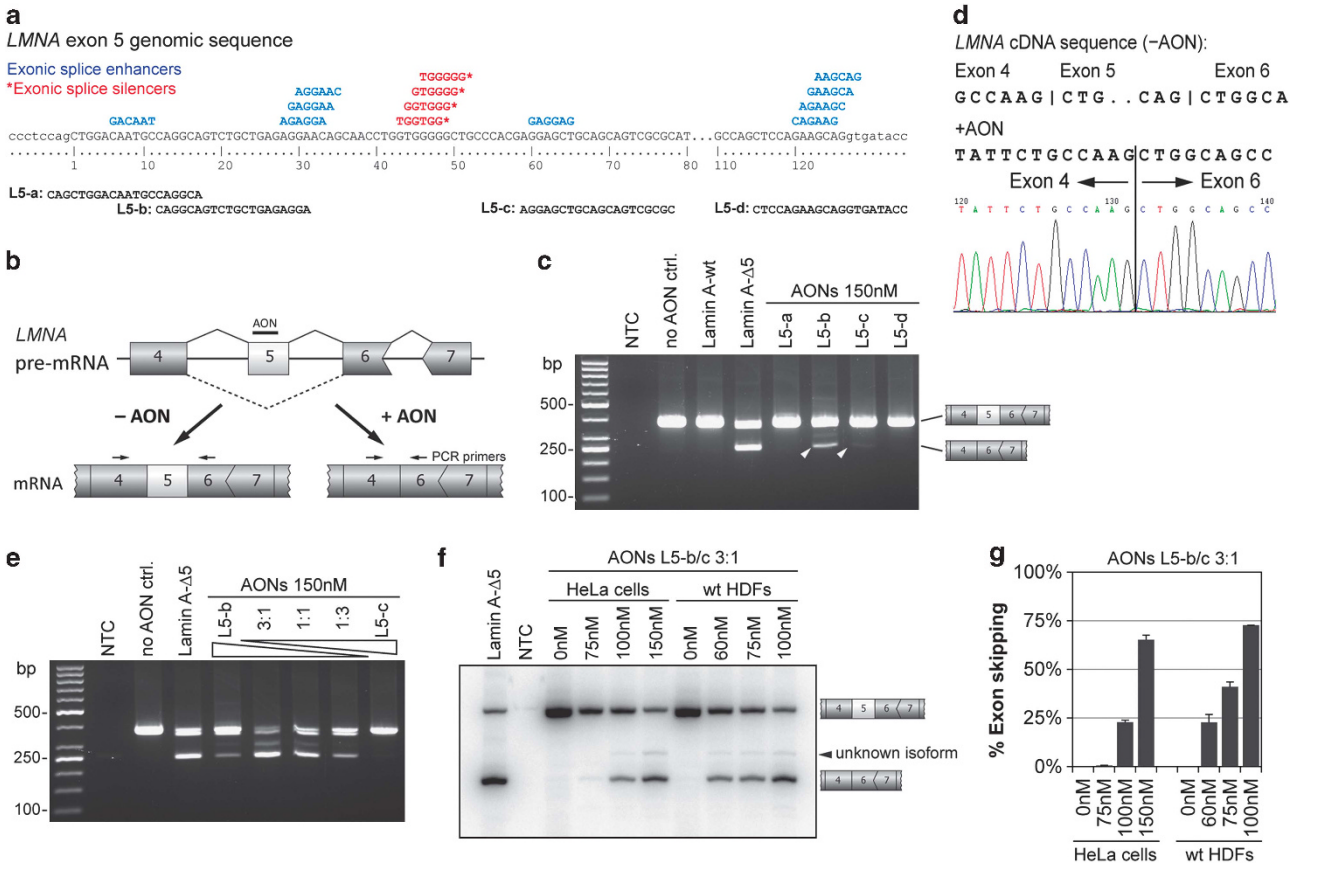

Figure 6. AONs targeting *LMNA*-exon 5 induce exon 5 exclusion in human cells. (**a**) *LMNA* exon structure indicating exon 5 sequence (upper case) with flanking intronic sequence (lower case). Exonic splice enhancer motifs (ESE, blue) and silencer motifs (ESS, red, marked by asterisk (*)) are indicated above the sequence. AON-target sites are indicated below labelled L5-a, L5-b, L5-c and L5-d. (**b**) The skipping efficacy of each AON was established using a PCR primer pair located on *LMNA* exons 4 and 6 to generate a 375-bp (full length) and 250-bp (skipped exon 5) amplicon. (**c**) HeLa cells transfected with L5-b and L5-c for 3 days induced skipping of exon 5, as revealed by the presence of the 250 bp amplicon (highlighted by arrowheads). Negative controls of no template control (NTC), no AON control and cells transfected with Lamin A-wt cDNA did not show the 250-bp band. For the positive size control, Lamin A-Δ5 encoding cDNA was transfected into the cells. (**d**) Correct splicing of mRNA lacking exon 5 was confirmed by sequencing. The full-length wild-type *LMNA* mRNA sequence, as well as the sequence lacking exon 5, are shown. The electropherogram confirms correct splicing of *LMNA* exons 4 and 6 in AON-treated HeLa cells. (**e**) Different ratios of the two effective AONs (L5-b and L5-c) were combined to determine if skipping efficacy could be improved, with L5-b/c mixed at a ratio of 3:1 being optimal. (**f**) *LMNA* exon 5 skipping efficiency was quantified by semi-quantitative radioactive PCR. HeLa cells and wild-type human dermal fibroblasts (wt HDFs) demonstrated a dose response when treated with increased AON concentrations (L5-b/c ratio 3:1). HeLa cells transfected with Lamin A-Δ5 encoding cDNA served as a size control (lane 1). (**g**) Relative mean ± s.e.m. percentage of *LMNA*-Δ5 compared with full-length *LMNA* was calculated using cytidine-content normalised intensity after radioactive PCR from three independent replicates.

Figure 5. Human Lamin C-Δ5 rescues nuclear abnormalities in *lmna*-null pMEFs. (**a**) Human Lamin C constructs were full-length wild-type lamin C (Lamin C-wt), Lamin C with the amino acids encoded by exon 3 deleted (Lamin C-Δ3) and Lamin C with the amino acids encoded by exon 5 deleted (Lamin C-Δ5). (**b**) Western blotting analysis of wild-type and *lmna*-null pMEFs infected with retroviruses encoding each of the Lamin C constructs shows that their sizes are correct, expression levels are consistent with endogenous Lamin A/C levels and production of eGFP from the *IRES-eGFP* in the retroviral backbone. β-Tubulin served as a loading control. (**c**) Representative micrographs of nuclei from eGFP +ve *lmna*-null pMEFs infected with retroviral constructs encoding different Lamin C variants immunostained for Lamin A/C. Lamin C-Δ5 localised correctly, whereas Lamin C-Δ3 shows marked abnormalities, including patchy staining (arrow) and aggregates (arrowhead). Inserts show DAPI-stained nuclei. (**d**) Mean percentage of eGFP+ve *lmna*-null MEFs that have a regular distribution of Lamin C throughout the nucleus and around the nuclear rim, as seen in *lmna*-null pMEFs expressing Lamin C-wt. Open circles represent values obtained from three independent *lmna*-null pMEF lines, with at least 299 nuclei in total analysed for each condition. (**e**) Representative micrographs of nuclei from eGFP+ve *lmna*-null MEFs infected with retroviral constructs encoding different Lamin C variants immunostained for endogenous Lamin B1. Lamin C-Δ5 localised Lamin B1 correctly, whereas abnormal Lamin B1 capping (arrows) and honeycomb structures (arrowheads) were seen with Lamin C-Δ3 expression. (**f**) Mean percentage of *lmna*-null MEFs that have a regular distribution of Lamin B1 throughout the nucleus and around the nuclear rim. Open circles represent values obtained from three independent *lmna*-null pMEF lines, with at least 360 nuclei analysed in total for each condition. (**g**) Representative micrographs of eGFP+ve infected *lmna*-null pMEFs co-immunostained for endogenous emerin. Infection with retroviruses encoding Lamin C-wt or Lamin C-Δ5 restored emerin distribution to the nucleus, but Lamin C-Δ3 was unable to normalise emerin localisation. (**h**) Average contour ratio of nuclei from eGFP+ve infected *lmna*-null pMEFs showed that Lamin C-Δ5 rescued nuclear shape, while Lamin C-Δ3 was unable to restore normal nuclear morphology. Open circles represent values obtained from three independent *lmna*-null pMEF lines, with at least 260 nuclei in total analysed for each condition. Significant difference from control retrovirus or Lamin C-wt infected cells as appropriate (Ref.) using a two-tailed paired *t*-test is denoted by $*P < 0.05$ or $**P < 0.01$, while 'NS' indicates no significant change.

the nuclear membrane in many eGFP+ve *lmna*-null pMEFs expressing Lamin C-wt or Lamin C-Δ5 but not with Lamin C-Δ3 (Figure 5g). Furthermore, nuclear morphology of *lmna*-null pMEFs was again improved by Lamin C-wt (CR 0.87) or Lamin C-Δ5 (CR 0.82) but not by Lamin C-Δ3 (CR 0.73), compared with RV control (CR 0.77) (Figure 5h).

AON-mediated exon skipping of *LMNA* exon 5 is feasible in human cells

We next determined whether it was feasible to target *LMNA* exon 5 for AON-mediated exon skipping in human cells. We designed 20mer 2′-O-methyl phosphorothioate AONs against four target regions in the *LMNA* gene, termed L5-a, L5-b, L5-c and L5-d, including exon–intron borders and exonic splice enhancers (ESEs—identified using the RESCUE-ESE web server[32]) but not exonic splice silencer (ESS—identified using the FAS-ESS web server[33]) (Figure 6a). Final AON target sites were selected considering additional criteria including GC-content and binding energy (calculated using RNA structure),[34] and taking into account secondary structure (accessibility) of the target site, as these factors are known to affect exon-skipping efficiency of the dystrophin transcript.[35] A scrambled AON control was not used as we were generating a novel *LMNA* transcript.

Exon skipping in AON-transfected HeLa cells was monitored by PCR using primers located in flanking *LMNA* exons 4 and 6, resulting in either a wild-type *LMNA* 376 bp amplicon or a 250 bp *LMNA*-Δ5 amplicon (Figures 6b and c). Only AONs targeting *LMNA* ESEs (L5-b and L5-c) induced exon skipping, with L5-b more efficient than L5-c (Figure 6c), consistent with observations that in some cases exon targeting AONs are more efficient at skipping *DMD* exons.[36,37] The two of the four AONs that failed to direct skipping of *LMNA* exon 5 (L5-a and L5-d) can also be regarded as negative controls. The 250-bp amplicon was sequenced, confirming correct splicing of *LMNA* exons 4–6 (Figure 6d). Primers located in *LMNA* exons 3 and 7 also generated two amplicons corresponding to either wild-type *LMNA* or *LMNA*-Δ5 transcripts (data not shown), confirming that splicing of adjacent exons was unaffected by AON treatment.

A synergistic effect can occur when AONs are used in combination in *DMD*.[38] AONs L5-b and L5-c used together resulted in dramatically increased *LMNA* exon-skipping efficiency at all tested ratios, with maximal exon skipping at a L5-b:L5-c ratio of 3:1 (Figure 6e). Thus synergy, rather than merely an additive effect, was achieved by simultaneously targeting two separate ESEs in *LMNA* exon 5 with specific AONs (Figure 6a).

We also confirmed that the AONs were effective at skipping *LMNA* exon 5 in primary 'wild-type' human dermal fibroblasts (wt-HDFs). Three days posttransfection with L5-b/L5-c in a ratio of 3:1, we observed a dose response of *LMNA* exon 5 skipping in both HeLa cells and wt-HDFs (Figure 6f). Quantification of relative isoform expression by radioactive PCR[6] confirmed the dose response, with a maximum relative mean ± s.e.m. skipping efficiency for *LMNA*-Δ5 transcript of 65.2 ± 2.4% for HeLa cells (at 150 nM AON) and 72.7 ± 0.02% in wt-HDFs (at 100 nM AON), compared with full-length *LMNA* transcript (Figure 6g).

DISCUSSION

Exon skipping is currently in clinical trials for DMD to correct a disrupted reading frame.[4] Here we explored expanding this RNA therapy to include diseases caused mainly by missense mutations: using laminopathies as our model. Human Lamin A or Lamin C with a deletion corresponding to amino acids encoded by exon 5 not only localised normally in murine *lmna*-null cells, but also restored both nuclear shape and localisation of endogenous Lamin B1 and emerin. In wild-type murine cells, human Lamin A/C-Δ5 did not cause any dominant deleterious phenotypes, in contrast to human Lamin A species with missense mutations in exon 5. It is feasible to use AONs to skip *LMNA* exon 5 in human cells, raising the possibility of transfer to clinical studies for laminopathies arising from mutations in this exon (Table 1). This is the first report, to our knowledge, of the potential use of exon skipping as a therapy for diseases arising from missense mutations.

Why then did Lamin A-Δ3 and Lamin C-Δ3 act in a dominant-negative manner? *LMNA* exon 3 encodes six heptad repeats in coil 1B, while exon 5 encodes six heptad repeats in coil 2B. However, the heptad repeats encoded by *LMNA* exon 5 start at position 'a', whereas those encoded by *LMNA* exon 3 begin at position 'd' (Figures 1b–c). Thus removal of amino acids encoded by *LMNA* exon 3 creates a shortened Lamin A/C protein containing a novel hybrid heptad at the new junction formed of amino acids encoded by exons 2 and 4. With removal of *LMNA* exon 5 encoded amino acids in contrast, the internally-truncated Lamin A/C simply has the native heptads encoded by exons 4 and 6, juxtaposed. Notably, the central rod domain of cytoplasmic intermediate filaments also lacks six heptad repeats in coil 1B, which mimics the protein structure attributed to Lamin A-Δ3 but not to Lamin A-Δ5 (Figure 1). Adding six further heptad repeats to neurofilament light affects its co-assembly with vimentin, leading to speculation that these extra repeats in nuclear lamins prevent them from associating with cytoplasmic intermediate filament proteins.[39] A protein similar to Lamin A-Δ3 is produced by removal of both six coil 1B heptad repeats and the CAAX motif from Lamin B, and this protein too, forms nuclear aggregates.[40] These observations also indicate that these additional six heptad repeats in coil 1B are not necessary for nuclear targeting of lamins but are needed for their proper localisation to the nuclear lamina. Lamin A-Δ3 therefore, may inefficiently/be unable to, assemble and integrate into the nuclear lamina formed by full-length A- and B-type lamins and so forms aggregates.

The net charge of amino acids encoded by *LMNA* exons 3 and 5 also differs, with the exon 3-encoded amino acids having a net charge of − 3, while those encoded by exon 5 have a net charge of +1. Loss of three negatives charges could have a stronger effect on homodimerisation and/or heterodimerisation, or interaction with Lamin A-binding partners such as SUN1, since deletion of the lamin A-binding site in SUN1 disrupts Lamin A/C localisation in mouse fibroblasts.[41] Other Lamin A interaction partners specifically bind to coil 1 (c-Fos[42]) or coil 2 (pRb, Erk1/2 and MOK2[43–45]). These binding partners are involved in nucleo-cytoskeletal signalling and thus deleting the Lamin A-binding site for c-Fos, in particular, appears detrimental.

Laminopathies are predominantly caused by autosomal-dominant missense mutations (http://www.umd.be/LMNA/). Genetic means to correct the pathogenic phenotype could embrace gene-editing techniques, including exon-exchange technologies such as spliceosome-mediated RNA trans splicing.[46] However, these technologies are still in their infancy and relatively inefficient. In contrast, exon skipping is in clinical trial for DMD to remove exons to restore the reading frame and has proven effective for producing semi-functional dystrophin.[3,4] Exon skipping has also been used for other applications, including correcting mis-splicing, switching alternative splicing, inducing gene knockdown and so on, but not to correct missense mutations.[47]

AONs can efficiently skip *LMNA* exon 5 in primary human cells, and so patients with mutations in exons 5 would potentially benefit from such a therapy. Twenty mutations in *LMNA* exon 5 have been reported, 14/20 of which are dominant missense and 5/20 nonsense mutations. The vast majority of these mutations are associated with neuromuscular disorders, including EDMD, LGMD1B, L-CMD and DCM. The remaining mutation (p.R298C), causes AR-CMT2A (http://www.umd.be/LMNA/) (Table 1).

Exon skipping in dominant mutations would not only reduce levels of pathogenic Lamin A/C species but also wild-type Lamin

A/C from the un-mutated allele. However, even complete replacement of all A-type lamins with Lamin A/C-Δ5 should be acceptable considering that human Lamin A/C-Δ5 alone can rescue murine *lmna*-null cells. Indeed, it is unknown by how much the amount of mutant Lamin A/C protein would need to be reduced from the presumed ~ 50% level in patients to ameliorate a pathogenic phenotype, and it is also likely to be mutation-dependent. Current exon-skipping technology is not efficient,[48] but modifications including AONs conjugated with cell-penetrating peptides that are cell-type specific to target, for example, skeletal[49] or cardiac muscle,[48] will further improve efficiency.

To treat laminopathies arising from recessive mutations, however, it is probable that only small amounts of Lamin A/C-Δ5 protein would be required to alleviate disease symptoms. A recessive mutation in exon 5 is p.R298C that causes AR-CMT2A: a peripheral neuropathy characterised by improper myelination and demyelination leading to axonal loss (Table 1).[50] Hence, targeting Schwann cells in peripheral nerve with AONs to skip exon 5 could be a potential treatment, with uptake of AONs into neuronal cell types already demonstrated in SMA mouse models.[6]

The next step is to test other AON sequences and backbone chemistries to better optimise exon-skipping delivery and efficiency. Ideally, this will then encompass trying to rescue pathogenic phenotypes in patient cells *in vitro*. Although rare, there are primary fibroblasts available carrying mutations in *LMNA* exon 5. We obtained primary human fibroblasts carrying p.L302P, which were isolated from a patient with L-CMD.[51] We found that initially, some of these cells had mislocalisation of Lamin A/C and Lamin B, although no overt nuclear morphology was noted. However, this phenotype was unstable, rapidly disappearing upon further culture (unpublished observations). Thus we are intending to generate induced pluripotent stem cells from p.L302P and other patient cells, to produce both sufficient cells for extensive AON testing and to differentiate into particular cell lineages to gauge tissue-specific effects of skipping *LMNA* exon 5.

To show phenotypic rescue of AONs *in vivo*, we require an animal model with a mutation in *Lmna* exon 5, and only one appropriate mouse has been reported: the AR-CMT2A model carrying the p.R298C missense mutation.[52] Unfortunately, however, despite exhaustive behavioural tests and histopathological analyses, no overt peripheral nerve phenotype was found in $Lmna^{R298C/R298C}$ mice, leaving us no means to measure rescue by administration of *lmna* exon 5 skipping AONs.

It would also be informative to test whether deleterious effects caused by missense mutations, insertions or deletions in other parts of Lamin A/C could also be ameliorated by deleting exon 5. Speculatively, a change in the structure of Lamin A/C caused by removing exon 5 and shortening the central rod domain may make this novel isoform interact differently with wild-type Lamin A/C. This altered interaction with wild-type Lamin A/C may then ameliorate the deleterious effects of mutations located in *LMNA* exons other than 5. Potential candidates could include mutations in the central rod domain that affect pitch of the α-helical coiled coil.

In conclusion, *LMNA* exon 5 presents a candidate for further investigation into exon-skipping therapy in laminopathies. Both human Lamin A-Δ5 and Lamin C-Δ5 localise normally in murine *lmna*-null pMEFs and can rescue nuclear abnormalities generally associated with laminopathies. We believe that this is the first evidence that missense mutations could be treated by simply removing the mutated exon. This opens the possibility that other proteins that contain similar repeating redundant units and are pathogenic when carrying missense, nonsense mutations or small duplication/deletions could also be treated by exon skipping. Thus these observations are of significantly wider clinical interest than simply as a potential treatment for laminopathies.

MATERIALS AND METHODS

Mice

Procedures were carried out under the Animals (Scientific Procedures) Act 1986. C57BL/6 $Lmna^{+/-}$ mice[26] were from Carlos Lopez-Otin (University of Oviedo, Oviedo, Spain) and genotyped as described.[53]

Retroviral vectors

Wild-type human Lamin A (Lamin A-wt)[16] and three human mutant Lamin A cDNAs were obtained in pEGFP-C1 (p.R190dup, p.S295P, p.S303P). Lamin A-N195K was created using the QuikChange Site-directed Mutagenesis Kit (Agilent Technologies, Santa Clara, CA, USA). Human Lamin A-Δ3 and Lamin A-Δ5 encoding cDNA were created by PCR. Human Lamin C-wt, Lamin C-Δ3 and Lamin C-Δ5 encoding cDNA were created by amplifying Lamin A-wt, Lamin A-Δ3 and Lamin A-Δ5 using a primer containing the Lamin C-specific C-terminal sequence VSGSRR*. All were cloned into *pMSCV-IRES-eGFP* and packaged using standard methods.[16]

Antisense oligonucleotides

2′O-methyl phosphorothioate AONs were purchased from IDT (Leuven, Belgium) and transfected using TurboFect transfection reagent (Thermo Scientific, Waltham, MA, USA) and analysed 72 h posttransfection.

Cell culture and retroviral infection

HeLa cells (ATCC, Manassas, VA, USA) were maintained in growth medium (Dulbecco's modified Eagle's medium/10% fetal bovine serum (GE Healthcare, Little Chalfont, UK)/2 mM Glutamine (Sigma-Aldrich, St Louis, MO, USA)). Primary wild-type human dermal fibroblasts were maintained in growth medium with 1% Penicillin/Streptomycin (Sigma-Aldrich). Primary murine embryonic fibroblasts (pMEFs) were obtained from 3 wild-type and 3 *lmna*-null embryos (13.5–14.5 dpc), and maintained in growth medium supplemented with 0.1 mM β-mercaptoethanol (Sigma-Aldrich). In all, 150 000 pMEFs per well of a six-well plate were exposed to retroviral supernatant (diluted 1:5 in growth medium with 4 μg ml^{-1} polybrene) for at least 6 h before analysis at 72–96 h postinfection.

Immunostaining

Cells were fixed with 4% paraformaldehyde/phosphate-buffered saline for 10 min, permeabilised with 0.5% Triton X-100/phosphate-buffered saline for 10 min and blocked with 5% goat/swine serum for 1 h at room temperature. Primary antibodies used were mouse anti-Lamin A/C 131C3 1:250; rabbit anti-Lamin B1 1:2000 (Abcam, Cambridge, UK); rabbit anti-emerin AP8 1:100[54] and chicken anti-GFP 1:2000 (Molecular Probes, Eugene, OR, USA). Primary antibody binding was revealed using Alexa Fluor-coupled secondary antibodies (1:500) (Molecular Probes) and DAPI (4,6-diamidino-2-phenylindole) counterstaining.

Morphometric/fluorescence analysis

Nuclei were outlined using the polygon selection tool, and perimeter and cross-sectional area were measured with NIH ImageJ (http://imagej.nih.gov/ij/) and the contour ratio calculated ($4\pi \times$ area/circumference^2).[16] A contour ratio of a circle is 1, and the value gets smaller with increasing deformation (Figure 2e). Representative nuclei stained for DAPI and immunostained for emerin were analysed using 'Plot Profile' in ImageJ.

Western blotting

Cells were lysed in 1× Laemmli sample buffer and immunoblotted with: goat anti-Lamin A/C N18 1:1000 (Santa Cruz Biotechnology, Santra Cruz, CA, USA), rabbit anti-GFP 1:2000 (Molecular Probes), and mouse anti-β-tubulin 1:1000 (DSHB, Iowa City, IA, USA); and then probed with horseradish peroxidase-conjugated secondary antibodies (ECL sheep anti-mouse or sheep anti-rabbit 1:5000 (GE Healthcare); rabbit anti-goat 1:50000, Abcam) and developed using enhanced chemiluminescence (GE Healthcare).

PCR and quantification of exon skipping

Total RNA was isolated using RNeasy spin columns (Qiagen, Venlo, the Netherlands) and reverse transcribed using the QuantiTect Reverse Transcription Kit (Qiagen). PCR was performed using either exon 4 Fwd 5′-CCAAGCGCCGTCATGAGACC-3′ and exon 6 Rev 5′-CGCTCCTTTTCCGC CAGCAG-3′ primers, resulting in a 376-bp amplicon (wild-type) and 250-bp amplicon (*LMNA*-Δ5), or exon 3 Fwd 5′-CTTCCAGAAGAACATCTACAGTG-3′

and exon 7 Rev 5′-AGGGCTGGGGGACAGGCGTAG-3′ resulting in a 565-bp amplicon (wild-type) and 439-bp amplicon (*LMNA*-Δ5). Semi-quantitative PCR was performed using Amplitaq polymerase (Applied Biosystems, Foster City, CA, USA) with [α-^{32}P]-dCTP and exon 4 Fwd and exon 6 Rev primers. After 26 cycles, amplicons were separated on a 5% native polyacrylamide gel, visualised by autoradiography on a Typhoon 9410 phosphoimager (GE Healthcare) and quantified using the Multi Gauge software v2.3 (Fujifilm, Tokyo, Japan). Relative percentage of *LMNA*-Δ5 compared with full-length *LMNA* was calculated using cytidine-content normalised intensity.

Statistical analysis

Data were analysed and graphs were produced using Microsoft Excel (Microsoft, Redmond, WA, USA). Figures were compiled in Adobe Photoshop CS4 (Adobe, San Jose, CA, USA) and Adobe Illustrator CS4. Paired Student's *t*-test was used to test statistical difference between samples at $*P < 0.05$ and $**P < 0.01$.

CONFLICT OF INTEREST

The authors declare no conflict of interest.

ACKNOWLEDGEMENTS

We thank Matthew Wood and his laboratory members for their advice. L302P human patient fibroblasts were a kind gift from Gisèle Bonne (Institute of Myology, Paris, France). JS and NF were partially funded by OPTISTEM (223098) through EU FP7. PSZ is also supported by The Muscular Dystrophy Campaign, the Medical Research Council (G1100193), Association Française contre les Myopathies and BIODESIGN (262948-2) through EU FP7.

REFERENCES

1 Dominski Z, Kole R. Restoration of correct splicing in thalassemic pre-mRNA by antisense oligonucleotides. *Proc Natl Acad Sci USA* 1993; **90**: 8673–8677.
2 Wilton SD, Lloyd F, Carville K, Fletcher S, Honeyman K, Agrawal S *et al.* Specific removal of the nonsense mutation from the mdx dystrophin mRNA using antisense oligonucleotides. *Neuromuscul Disord* 1999; **9**: 330–338.
3 Mendell JR, Rodino-Klapac LR, Sahenk Z, Roush K, Bird L, Lowes LP *et al.* Eteplirsen for the treatment of Duchenne muscular dystrophy. *Ann Neurol* 2013; **74**: 637–647.
4 Cirak S, Arechavala-Gomeza V, Guglieri M, Feng L, Torelli S, Anthony K *et al.* Exon skipping and dystrophin restoration in patients with Duchenne muscular dystrophy after systemic phosphorodiamidate morpholino oligomer treatment: an open-label, phase 2, dose-escalation study. *Lancet* 2011; **378**: 595–605.
5 Muntoni F, Torelli S, Ferlini A. Dystrophin and mutations: one gene, several proteins, multiple phenotypes. *Lancet Neurol* 2003; **2**: 731–740.
6 Hua Y, Sahashi K, Rigo F, Hung G, Horev G, Bennett CF *et al.* Peripheral SMN restoration is essential for long-term rescue of a severe spinal muscular atrophy mouse model. *Nature* 2011; **478**: 123–126.
7 Kole R, Krainer AR, Altman S. RNA therapeutics: beyond RNA interference and antisense oligonucleotides. *Nat Rev Drug Discov* 2012; **11**: 125–140.
8 Vanderplanck C, Ansseau E, Charron S, Stricwant N, Tassin A, Laoudj-Chenivesse D *et al.* The FSHD atrophic myotube phenotype is caused by DUX4 expression. *PloS one* 2011; **6**: e26820.
9 Worman HJ, Bonne G. "Laminopathies": a wide spectrum of human diseases. *Exp Cell Res* 2007; **313**: 2121–2133.
10 Scharner J, Gnocchi VF, Ellis JA, Zammit PS. Genotype-phenotype correlations in laminopathies: how does fate translate? *Biochem Soc Trans* 2010; **38**: 257–262.
11 Bonne G, Di Barletta MR, Varnous S, Becane HM, Hammouda EH, Merlini L *et al.* Mutations in the gene encoding lamin A/C cause autosomal dominant Emery-Dreifuss muscular dystrophy. *Nat Genet* 1999; **21**: 285–288.
12 Stuurman N, Heins S, Aebi U. Nuclear lamins: their structure, assembly, and interactions. *J Struct Biol* 1998; **122**: 42–66.
13 Dechat T, Adam SA, Taimen P, Shimi T, Goldman RD. Nuclear lamins. *Cold Spring Harb Perspect Biol* 2010; **2**: a000547.
14 Davidson PM, Lammerding J. Broken nuclei--lamins, nuclear mechanics, and disease. *Trends Cell Biol* 2014; **24**: 247–256.
15 Burke B, Stewart CL. Life at the edge: the nuclear envelope and human disease. *Nat Rev Mol Cell Biol* 2002; **3**: 575–585.
16 Scharner J, Brown CA, Bower M, Iannaccone ST, Khatri IA, Escolar D *et al.* Novel LMNA mutations in patients with Emery-Dreifuss muscular dystrophy and functional characterization of four LMNA mutations. *Hum Mutat* 2011; **32**: 152–167.
17 de Las Heras JI, Meinke P, Batrakou DG, Srsen V, Zuleger N, Kerr AR *et al.* Tissue specificity in the nuclear envelope supports its functional complexity. *Nucleus* 2013; **4**: 460–477.
18 Scharner J, Lu HC, Fraternali F, Ellis JA, Zammit PS. Mapping disease-related missense mutations in the immunoglobulin-like fold domain of lamin A/C reveals novel genotype-phenotype associations for laminopathies. *Proteins* 2014; **82**: 904–915.
19 Cao K, Graziotto JJ, Blair CD, Mazzulli JR, Erdos MR, Krainc D *et al.* Rapamycin reverses cellular phenotypes and enhances mutant protein clearance in Hutchinson-Gilford progeria syndrome cells. *Sci Transl Med* 2011; **3**: 89ra58.
20 Gordon LB, Kleinman ME, Miller DT, Neuberg DS, Giobbie-Hurder A, Gerhard-Herman M *et al.* Clinical trial of a farnesyltransferase inhibitor in children with Hutchinson-Gilford progeria syndrome. *Proc Natl Acad Sci USA* 2012; **109**: 16666–16671.
21 Muchir A, Shan J, Bonne G, Lehnart SE, Worman HJ. Inhibition of extracellular signal-regulated kinase signaling to prevent cardiomyopathy caused by mutation in the gene encoding A-type lamins. *Hum Mol Genet* 2009; **18**: 241–247.
22 Liu GH, Suzuki K, Qu J, Sancho-Martinez I, Yi F, Li M *et al.* Targeted gene correction of laminopathy-associated LMNA mutations in patient-specific iPSCs. *Cell Stem Cell* 2011; **8**: 688–694.
23 Cohen TV, Gnocchi VF, Cohen JE, Phadke A, Liu H, Ellis JA *et al.* Defective skeletal muscle growth in lamin A/C-deficient mice is rescued by loss of Lap2alpha. *Hum Mol Genet* 2013; **22**: 2852–2869.
24 Scaffidi P, Misteli T. Reversal of the cellular phenotype in the premature aging disease Hutchinson-Gilford progeria syndrome. *Nat Med* 2005; **11**: 440–445.
25 van Engelen BG, Muchir A, Hutchison CJ, van der Kooi AJ, Bonne G, Lammens M. The lethal phenotype of a homozygous nonsense mutation in the lamin A/C gene. *Neurology* 2005; **64**: 374–376.
26 Sullivan T, Escalante-Alcalde D, Bhatt H, Anver M, Bhat N, Nagashima K *et al.* Loss of A-type lamin expression compromises nuclear envelope integrity leading to muscular dystrophy. *J Cell Biol* 1999; **147**: 913–920.
27 Mounkes LC, Kozlov S, Hernandez L, Sullivan T, Stewart CL. A progeroid syndrome in mice is caused by defects in A-type lamins. *Nature* 2003; **423**: 298–301.
28 Navarro CL, De Sandre-Giovannoli A, Bernard R, Boccaccio I, Boyer A, Genevieve D *et al.* Lamin A and ZMPSTE24 (FACE-1) defects cause nuclear disorganization and identify restrictive dermopathy as a lethal neonatal laminopathy. *Hum Mol Genet* 2004; **13**: 2493–2503.
29 Shumaker DK, Lopez-Soler RI, Adam SA, Herrmann H, Moir RD, Spann TP *et al.* Functions and dysfunctions of the nuclear lamin Ig-fold domain in nuclear assembly, growth, and Emery-Dreifuss muscular dystrophy. *Proc Natl Acad Sci USA* 2005; **102**: 15494–15499.
30 Vaughan A, Alvarez-Reyes M, Bridger JM, Broers JL, Ramaekers FC, Wehnert M *et al.* Both emerin and lamin C depend on lamin A for localization at the nuclear envelope. *J Cell Sci* 2001; **114**: 2577–2590.
31 Jung HJ, Coffinier C, Choe Y, Beigneux AP, Davies BS, Yang SH *et al.* Regulation of prelamin A but not lamin C by miR-9, a brain-specific microRNA. *Proc Natl Acad Sci USA* 2012; **109**: E423–E431.
32 Fairbrother WG, Yeh RF, Sharp PA, Burge CB. Predictive identification of exonic splicing enhancers in human genes. *Science* 2002; **297**: 1007–1013.
33 Wang Z, Rolish ME, Yeo G, Tung V, Mawson M, Burge CB. Systematic identification and analysis of exonic splicing silencers. *Cell* 2004; **119**: 831–845.
34 Reuter JS, Mathews DH. RNAstructure: software for RNA secondary structure prediction and analysis. *BMC Bioinformatics* 2010; **11**: 129.
35 Aartsma-Rus A, van Vliet L, Hirschi M, Janson AA, Heemskerk H, de Winter CL *et al.* Guidelines for antisense oligonucleotide design and insight into splice-modulating mechanisms. *Mol Ther* 2009; **17**: 548–553.
36 Aartsma-Rus A, Houlleberghs H, van Deutekom JC, van Ommen GJ, t Hoen PA. Exonic sequences provide better targets for antisense oligonucleotides than splice site sequences in the modulation of Duchenne muscular dystrophy splicing. *Oligonucleotides* 2010; **20**: 69–77.
37 Aartsma-Rus A, Janson AA, Kaman WE, Bremmer-Bout M, den Dunnen JT, Baas F *et al.* Therapeutic antisense-induced exon skipping in cultured muscle cells from six different DMD patients. *Hum Mol Genet* 2003; **12**: 907–914.
38 Adams AM, Harding PL, Iversen PL, Coleman C, Fletcher S, Wilton SD. Antisense oligonucleotide induced exon skipping and the dystrophin gene transcript: cocktails and chemistries. *BMC Mol Biol* 2007; **8**: 57.
39 Monteiro MJ, Hicks C, Gu L, Janicki S. Determinants for intracellular sorting of cytoplasmic and nuclear intermediate filaments. *J Cell Biol* 1994; **127**: 1327–1343.
40 Mical TI, Monteiro MJ. The role of sequences unique to nuclear intermediate filaments in the targeting and assembly of human lamin B: evidence for lack of interaction of lamin B with its putative receptor. *J Cell Sci* 1998; **111**: 3471–3485.
41 Haque F, Mazzeo D, Patel JT, Smallwood DT, Ellis JA, Shanahan CM *et al.* Mammalian SUN protein interaction networks at the inner nuclear membrane and their role in laminopathy disease processes. *J Biol Chem* 2010; **285**: 3487–3498.

42 Ivorra C, Kubicek M, Gonzalez JM, Sanz-Gonzalez SM, Alvarez-Barrientos A, O'Connor JE *et al*. A mechanism of AP-1 suppression through interaction of c-Fos with lamin A/C. *Genes Dev* 2006; **20**: 307–320.
43 Dreuillet C, Tillit J, Kress M, Ernoult-Lange M. In vivo and in vitro interaction between human transcription factor MOK2 and nuclear lamin A/C. *Nucleic Acids Res* 2002; **30**: 4634–4642.
44 Gonzalez JM, Navarro-Puche A, Casar B, Crespo P, Andres V. Fast regulation of AP-1 activity through interaction of lamin A/C, ERK1/2, and c-Fos at the nuclear envelope. *J Cell Biol* 2008; **183**: 653–666.
45 Ozaki T, Saijo M, Murakami K, Enomoto H, Taya Y, Sakiyama S. Complex formation between lamin A and the retinoblastoma gene product: identification of the domain on lamin A required for its interaction. *Oncogene* 1994; **9**: 2649–2653.
46 Puttaraju M, Jamison SF, Mansfield SG, Garcia-Blanco MA, Mitchell LG. Spliceosome-mediated RNA trans-splicing as a tool for gene therapy. *Nat Biotechnol* 1999; **17**: 246–252.
47 van Roon-Mom WM, Aartsma-Rus A. Overview on applications of antisense-mediated exon skipping. *Methods Mol Biol* 2012; **867**: 79–96.
48 Yin H, Moulton HM, Betts C, Seow Y, Boutilier J, Iverson PL *et al*. A fusion peptide directs enhanced systemic dystrophin exon skipping and functional restoration in dystrophin-deficient mdx mice. *Hum Mol Genet* 2009; **18**: 4405–4414.
49 Yin H, Moulton HM, Seow Y, Boyd C, Boutilier J, Iverson P *et al*. Cell-penetrating peptide-conjugated antisense oligonucleotides restore systemic muscle and cardiac dystrophin expression and function. *Hum Mol Genet* 2008; **17**: 3909–3918.
50 De Sandre-Giovannoli A, Chaouch M, Kozlov S, Vallat JM, Tazir M, Kassouri N *et al*. Homozygous defects in LMNA, encoding lamin A/C nuclear-envelope proteins, cause autosomal recessive axonal neuropathy in human (Charcot-Marie-Tooth disorder type 2) and mouse. *Am J Hum Genet* 2002; **70**: 726–736.
51 Quijano-Roy S, Mbieleu B, Bonnemann CG, Jeannet PY, Colomer J, Clarke NF *et al*. De novo LMNA mutations cause a new form of congenital muscular dystrophy. *Ann Neurol* 2008; **64**: 177–186.
52 Poitelon Y, Kozlov S, Devaux J, Vallat JM, Jamon M, Roubertoux P *et al*. Behavioral and molecular exploration of the AR-CMT2A mouse model Lmna (R298C/R298C). *Neuromolecular Med* 2012; **14**: 40–52.
53 Gnocchi VF, Scharner J, Huang Z, Brady K, Lee JS, White RB *et al*. Uncoordinated transcription and compromised muscle function in the lmna-null mouse model of Emery- Emery-Dreyfuss muscular dystrophy. *PLoS One* 2011; **6**: e16651.
54 Ellis JA, Craxton M, Yates JR, Kendrick-Jones J. Aberrant intracellular targeting and cell cycle-dependent phosphorylation of emerin contribute to the Emery-Dreifuss muscular dystrophy phenotype. *J Cell Sci* 1998; **111**: 781–792.
55 Strelkov SV, Schumacher J, Burkhard P, Aebi U, Herrmann H. Crystal structure of the human lamin A coil 2B dimer: implications for the head-to-tail association of nuclear lamins. *J Mol Biol* 2004; **343**: 1067–1080.
56 Herrmann H, Aebi U. Intermediate filaments: molecular structure, assembly mechanism, and integration into functionally distinct intracellular Scaffolds. *Annu Rev Biochem* 2004; **73**: 749–789.